

Continuous-wave laser generated jets for needle free applications

Carla Berrospe-Rodriguez, Claas Willem Visser, Stefan Schlautmann, Ruben Ramos-Garcia, and David Fernandez Rivas

Citation: *Biomicrofluidics* **10**, 014104 (2016); doi: 10.1063/1.4940038

View online: <http://dx.doi.org/10.1063/1.4940038>

View Table of Contents: <http://scitation.aip.org/content/aip/journal/bmf/10/1?ver=pdfcov>

Published by the **AIP Publishing**

Articles you may be interested in

[Thermally multiplexed polymerase chain reaction](#)

Biomicrofluidics **9**, 044117 (2015); 10.1063/1.4928486

[Microfluidic sorting of protein nanocrystals by size for X-ray free-electron laser diffraction](#)

Struct. Dyn. **2**, 041719 (2015); 10.1063/1.4928688

[Increasing label-free stem cell sorting capacity to reach transplantation-scale throughput](#)

Biomicrofluidics **8**, 064106 (2014); 10.1063/1.4902371

[Parallel generation of uniform fine droplets at hundreds of kilohertz in a flow-focusing module](#)

Biomicrofluidics **7**, 034112 (2013); 10.1063/1.4811276

[Biochip/laser cell deposition system to assess polarized axonal growth from single neurons and neuron/glia pairs in microchannels with novel asymmetrical geometries](#)

Biomicrofluidics **5**, 013408 (2011); 10.1063/1.3552998

AIP | **APL Photonics**

APL Photonics is pleased to announce
Benjamin Eggleton as its Editor-in-Chief



Continuous-wave laser generated jets for needle free applications

Carla Berrospe-Rodriguez,^{1,a)} Claas Willem Visser,² Stefan Schlautmann,³ Ruben Ramos-Garcia,¹ and David Fernandez Rivas³

¹*Departamento de Óptica, Instituto Nacional de Astrofísica, Óptica y Electrónica, Apartado Postal 51 y 216, 72000 Puebla, Pue., Mexico*

²*Physics of Fluids Group, MESA+ Institute and Faculty of Science and Technology, University of Twente, P.O. Box 217, 7500 AE Enschede, The Netherlands*

³*Mesoscale Chemical Systems Group, MESA+ Institute and Faculty of Science and Technology, University of Twente, P.O. Box 217, 7500 AE Enschede, The Netherlands*

(Received 10 November 2015; accepted 5 January 2016; published online 13 January 2016)

We designed and built a microfluidic device for the generation of liquid jets produced by thermocavitation. A continuous wave (CW) laser was focused inside a micro-chamber filled with a light-absorbing solution to create a rapidly expanding vapor bubble. The chamber is connected to a micro-channel which focuses and ejects the liquid jet through the exit. The bubble growth and the jet velocity were measured as a function of the devices geometry (channel diameter D and chamber width A). The fastest jets were those for relatively large chamber size with respect to the channel diameter. Elongated and focused jets up to 29 m/s for a channel diameter of 250 μm and chamber size of 700 μm were obtained. The proposed CW laser-based device is potentially a compact option for a practical and commercially feasible needle-free injector. © 2016 AIP Publishing LLC.

[<http://dx.doi.org/10.1063/1.4940038>]

I. INTRODUCTION

Needle injection has been the main drug delivery mechanism for nearly two centuries. However, needles constitute serious health problems such as inadequate disposal, waste contamination, and risk of infection.¹ In particular, they present a great danger for health care workers worldwide. It is estimated that nearly 2×10^6 of them experiences needle-stick incidences each year, which puts them at risk of diseases such as AIDS (Acquired Immune Deficiency Syndrome) and hepatitis, among others.^{2,3} Pain and needle-phobia are also problematic issues since patients avoid medical care for these reasons.⁴

Nowadays, there are several needle-free systems aimed at solving the problems mentioned above.⁵ Commercial systems include jet injectors,^{6–12} powder injectors,^{13,14} or monolithic formulations.¹⁵ Moreover, topical applications like thermal ablation^{16,17} and ultrasound,¹⁸ as well as micro-needle mechanisms,^{19–21} are still under development phase. Each system solves a challenge while having particular disadvantages; for example, liquid injectors can cause nozzle splash-back contamination from the skin; powder injectors can burn and bleach the skin; despite being painless, microneedles do not solve waste contamination problem and spreading of diseases.^{22,23}

Recently, fast liquid microjets were generated by the expansion of a vapor bubble induced by a focused pulsed laser. These jets have been studied as potentially efficient drug delivery system. Microjets with velocities above 200 m/s and penetration depths up to 4 mm have been reported.^{24,25} Such systems possess a kinematic focusing of the liquid with a sharp tip, preventing back-splash contamination. However, the laser is absorbed by the medicine-containing liquid, and therefore probably affects the chemistry of the injected material in an undesired

^{a)}Electronic mail: cberrospe@inaoep.mx

manner. Another pulsed laser-based jet injector with speeds up to 50 m/s and volume of 2100 nL has been developed to prevent this issue.^{26–30} Here, the container where cavitation occurs, and the nozzle where the drug is stored, were separated by a thermal resistant membrane.

Although these investigations hold promising results for needle free technology, the use of pulsed laser as cavitation source delays the development of inexpensive and portable devices. The dimensions of the commonly used Nd:YAG or Er:YAG lasers are impractically large, besides the requirement of a cooling system and a powerful source. Even though some pulsed laser systems are now more compact, they are still too large to integrate in portable devices, unlike near infrared (NIR) semiconductor laser with relatively high power. Furthermore, pulsed lasers are more expensive than continuous wave (CW) lasers since they require advanced optics and the use of special materials.

Therefore, to exploit the full benefits of laser-based injector, their cost, volume, and operation facilities need to be reduced. In fact, CW lasers have this potential. Liquid elongated jets were obtained focusing a CW laser into a droplet of copper nitrate saturated solution.³¹ However, the jet speed (≤ 10 m/s) was still insufficient to cross the skin barrier (stratum corneum).²⁷

In this work we present, to the best of our knowledge, the first microfluidic device to produce elongated liquid jets by CW-laser induced thermocavitation with speeds above the threshold to break the stratum corneum (outermost epidermal layer), which is the major barrier to chemical transfer through the skin. For a typical skin strength of 20 MPa, a minimum jet velocity of 14 m/s is needed.²⁷ The device focuses the bubble expansion with a specially designed geometry, leading to a liquid jet of 29 m/s. Thermocavitation produces jet speeds comparable with those by pulsed laser, opening the possibility to develop an inexpensive portable and needle free injector.

II. MATERIALS AND METHODS

A. Microfluidic cavity design and fabrication

Microfluidic devices were designed and fabricated in silicon and glass substrates under clean-room conditions. The samples are constituted by two parts: the chamber (where the cavitation bubble expands) and the channel (for liquid propagation and confinement), as shown in Figure 1(a). The device was fabricated with two different materials due to design characteristics. The chamber was etched in glass because isotropic etching allows fabrication of spherical-like geometries and optical access. This shape is important to allow bubble expansion but also to focus the shock waves at the channel entrance. On the other hand, silicon is a suitable material to use for straight channel fabrication.

Microchannels were micro-machined on double-side polished silicon wafers with (100) crystallographic orientation (SCHOTT MEMpax, Schott AG). The silicon channels with 500 μm length and a diameter of D were etched by means of a plasma dry-etching machine (Adixen AMS 100 SE, Alcatel). The glass substrates were made of Borofloat wafers, on which the chamber was wet-etched with hydrogen fluoride solutions. A chamber with 200 μm depth and a length of A was designed to allow the bubble to expand after its creation. Both substrates were put together with anodic bonding. The bonded wafers were then diced in square chips with a side of 10 mm.

The glass-silicon interface was chosen to avoid energy dispersion due to material deformation and surface detachment, as, for example, in polymer materials, such as Polydimethylsiloxane (PDMS).^{32,33} Furthermore, their low cost and ease of production with microfabrication techniques are additional advantages.

The geometrical parameters were classified by the chamber width A and the channel diameter D . For example, $A700D250$ represents a device with $A = 700 \mu\text{m}$ and $D = 250 \mu\text{m}$.

B. Optical setup

The setup depicted in Figure 1(b) was used to study the formation and growth of the bubble. An infrared collimated tunable laser, operating at $\lambda = 790 \text{ nm}$, was focused at the bottom of

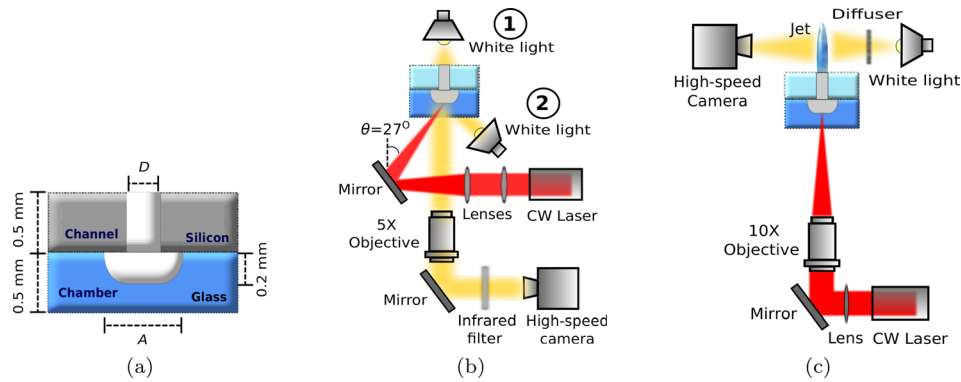


FIG. 1. (a) Artistic representation of the glass-silicon device cross section, geometry designed for thermocavitation jets experiments. The device is axisymmetric. (b) Setup for the bubble growth visualization inside the chamber device for top and bottom illumination. (c) Setup for the visualization of the jet.

the chamber with a 100 mm concave lens. Due to visualization limitations, the lens was oriented at 27° with respect to the device normal. The tilted focusing turns in to an angle of 18° inside the surface, as a consequence of light refraction, producing a slightly asymmetric superheated volume. However, once the bubble is created, its expansion becomes symmetric. With this configuration, it was possible to record the dynamics of the bubble wall inside the chamber. The device was illuminated by a white light source (Olympus ILP-1) located either at the top or the bottom from the channel and chamber, respectively. The bubble expansion was recorded at 54 000 frames per second (fps) with a $5\times$ microscope objective coupled to a fast camera (FASTCAM SA-X2 Photron) by a plane mirror. An infrared filter was used to avoid saturation of the CCD camera.

In each experiment, the chamber was filled by depositing a $25\ \mu\text{l}$ drop of copper nitrate saturated solution (13.78 g in 10 ml of water) at the exit of the device, with an optical absorption coefficient of $130\ \text{cm}^{-1}$ for the wavelength used. The device was then placed into a vacuum machine to introduce the liquid inside of the cavity, avoiding the formation of air bubbles in the chamber. With the help of a microscope, the residual solution outside the channel was removed with the tip of an absorbing tissue until the level was just below the channel exit.

The recordings of the liquid jet ejection from the channel were performed with the setup depicted in Figure 1(c). The laser was focused with a $10\times$ microscope objective producing a beam waist of $17\ \mu\text{m}$ (FWHM: Full width at half-maximum criteria) at the bottom of the chamber. The light source and the camera were located at the exit of the channel to observe the jet propagation. The image sequences were recorded at 180 000 fps. In order to capture the cavitation event in both experimental set-ups, a function generator was used to synchronize the laser with the camera by a trigger impulse of $\tau = 500\ \text{ms}$. During each laser illumination time, the liquid was superheated, a bubble was created, and as it expanded, liquid was pushed out of the channel. The expulsion of the jet could be repeated at least six times before the cavity was completely emptied. The results presented in this work all correspond to the first cavitation event.

For both experimental set-ups (bubble expansion and jet propagation), the device was placed in a holder with a xyz linear translation stage (micrometer precision) to align the center of the chamber with the center of the white light source, which was at the same time aligned with the spot of the infrared laser.

III. RESULTS AND DISCUSSION

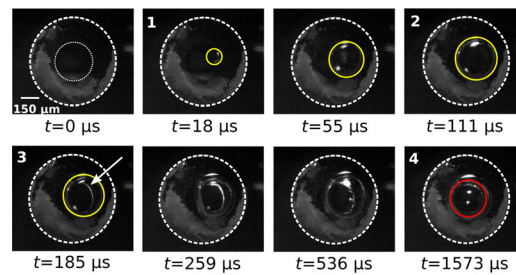
Due to the absorption of laser light at the bottom wall of the device, the liquid is heated up to its superheat limit ($270\text{--}300^\circ\text{C}$), leading to an explosive phase transition. As a consequence, a half-hemispheric bubble in contact with the chamber surface is created.^{34,35} The expansion of

the bubble causes the displacement of the liquid outside of the device, through the channel, in the form of a jet.

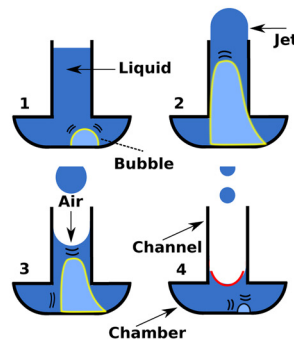
In order to understand and quantify the mechanism of jet production, the bubble growth and jet formation were analyzed as explained afterwards. The data points and the error bars plotted below represent the mean value of a total of four measurements (with variations smaller than 10%) and the uncertainty of these measurements, respectively.

A. Bubble dynamics inside the cavity

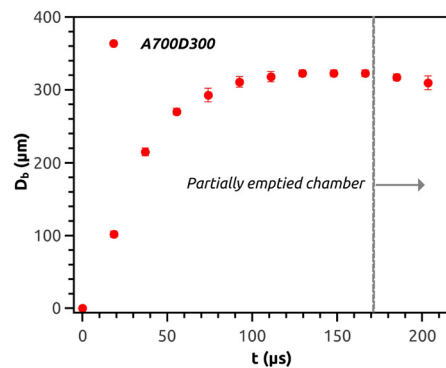
The dynamics of bubble expansion was recorded with bottom illumination, as shown in Figure 2(a). Initially, the bubble reaches a maximum diameter in the chamber at $t = 111 \mu\text{s}$; however, it continues growing along the channel, reaching a maximum size at $t = 185 \mu\text{s}$. This can be noticed since the top of the channel is visible, indicated by the white arrow. Due to the



(a)



(b)



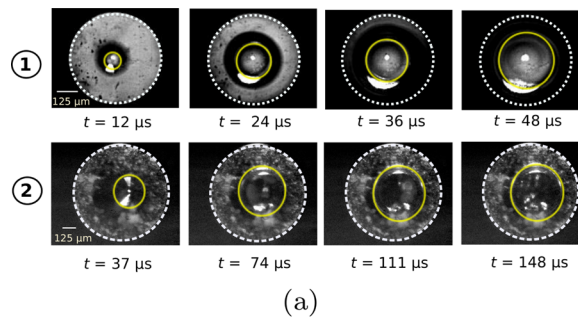
(c)

FIG. 2. (a) Bubble expansion inside the chamber for the device A700D300: bottom illumination. The dashed and dotted white circle delimits the area of the chamber and channel, respectively. The yellow continuous circle indicates the bubble wall and the red continuous circle the partially emptied chamber. (b) Artistic representation of the cross section for the bubble dynamics. (c) Bubble diameter growth as a function of time for laser intensity $I = 1.5 \times 10^4 \text{ W/cm}^2$.

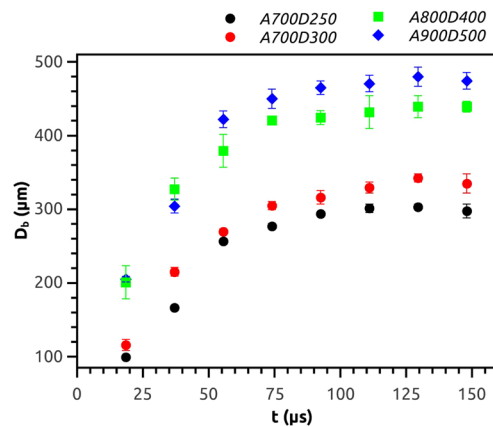
device configuration, the collapse of the bubble is not observable in the optical setup. In fact, what it is being observed at $t = 1573 \mu\text{s}$ is the partially emptied channel, as the air replaces the expelled liquid. The bubble dynamics is better understood looking at the artistic representation in Figure 2(b).

The bubble expansion in the chamber as a function of time, obtained from the image sequence of Figure 2(a), is shown in Figure 2(c). The main bubble growth occurs along the channel, producing a water jet expelled at different speeds as is shown later. After $t = 185 \mu\text{s}$, the diameter decreases, which may indicate the collapse of the bubble; however, it was not possible to measure the whole event due to the device configuration, as referred to above.

The influence of the geometrical design parameters, such as chamber A and channel width D , on the dynamics and size of the bubble were further investigated. The bubble expansion in time for different devices, presented in Figure 3(b), was obtained from image sequences as the one shown in Figure 3(a). The diameter of the bubble in the chamber was measured until its maximum value was reached. In all geometries, a faster growth occurs during the first $55 \mu\text{s}$ approximately, followed by slower expansion as a result of liquid ejection. Despite having space to expand in the chamber, in all the cases, the maximum bubble diameter was approximately the same size as the channel width. This is due to the main expansion occurring along the channel. However, the growth rate is proportional to the chamber width, the bigger the chamber, the faster the bubble grows. The bubble lifetime increases by decreasing the chamber width, similar to the results reported in literature.³⁶



(a)



(b)

FIG. 3. (a) Bubble expanding inside the chamber device *A900D500*: 1. Top illumination and 2. Bottom illumination. The white dotted and dashed circle delimits the area of the channel and chamber, respectively. The yellow continuous circle delimits the outer edge of the bubble. (b) Bubble diameter expansion against time for laser intensity $I = 1.5 \times 10^4 \text{ W/cm}^2$ until it reaches a maximum size in the chamber.).

B. Jet formation by thermocavitation

Initial dynamics of the jet produced by the bubble growth for different channel widths are shown in Figure 4(a). The image sequences present a common characteristic: a focused geometry (cone shaped) of the fluid is observed. In all cases, the tip of the jet is smaller than the channel width, indicated by the broken lines at the bottom of the jet. As it grows, the jet adopts the shape of a uniform cylindrical column. Sharper jet tips are observed for smaller channels. In particular, for *A700D250* (Figure 4(a-iii)), the angle is steep, and the liquid is almost a column from the beginning. It is expected that the increase in tip sharpness for smaller channels was caused by the increased curvature of the free surface, similar to previous results reported.²⁴ However, due to the lack of visualization of the meniscus in the silicon channel, future research will be required to validate this mechanism.

The propagation of the liquid jet for times after $100\ \mu\text{s}$ is shown in Figure 4(b). An elongated liquid column is observed after its formation at $312\ \mu\text{s}$. Before $702\ \mu\text{s}$ of propagation, the jet column reaches its maximum size and breaks into droplets from the back of the tip in the direction of jet displacement. In this particular case, the length of the jet before its break up was more than 3.5 mm.

The jet velocity as a function of time for different devices is presented in Figure 5(a). The speed increases as the channel diameter decreases; for *A800D300*, a maximum velocity of 27.5 m/s was measured, while for *A800D400*, it was 20.5 m/s. In all the devices, the speed of the liquid decreases rapidly within the first $16\ \mu\text{s}$, decaying slower afterwards and reaching a constant value around $25\ \mu\text{s}$ of propagation. For smaller channels, the jet decelerates more rapidly because there is more resistance to flow.

The effect of the chamber width on the jet velocity is shown in Figure 5(b). For devices with the same channel dimensions, a faster jet is observed for bigger chambers. As was

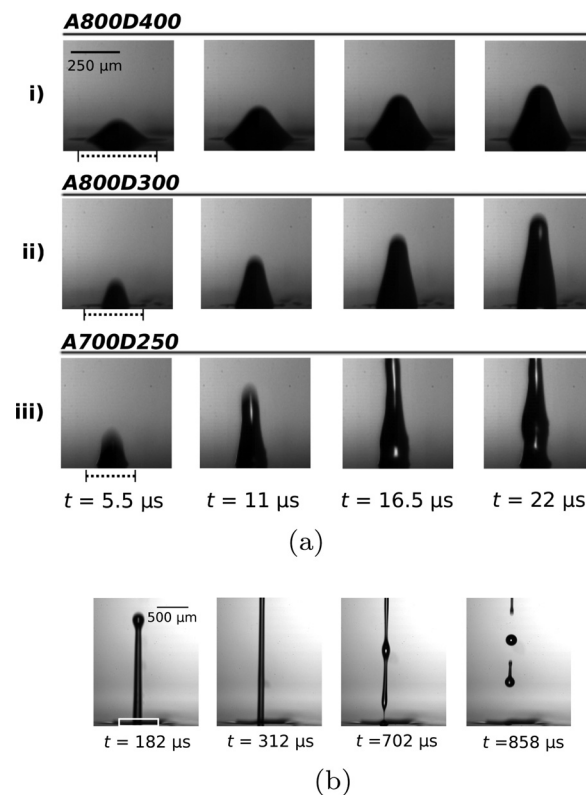


FIG. 4. Image sequences recorded at 180 000 fps for liquid jets generated with laser intensity $I = 2.6 \times 10^4\ \text{W/cm}^2$, as a consequence of the bubble growth in the chamber. At $16.5\ \mu\text{s}$ of propagation, the tip of the jet from *A700D250* is already out of the field of view. (b) Propagation of the jet after its formation. Break-up of the liquid column at $t = 702\ \mu\text{s}$ and droplet formation at $t = 858\ \mu\text{s}$.

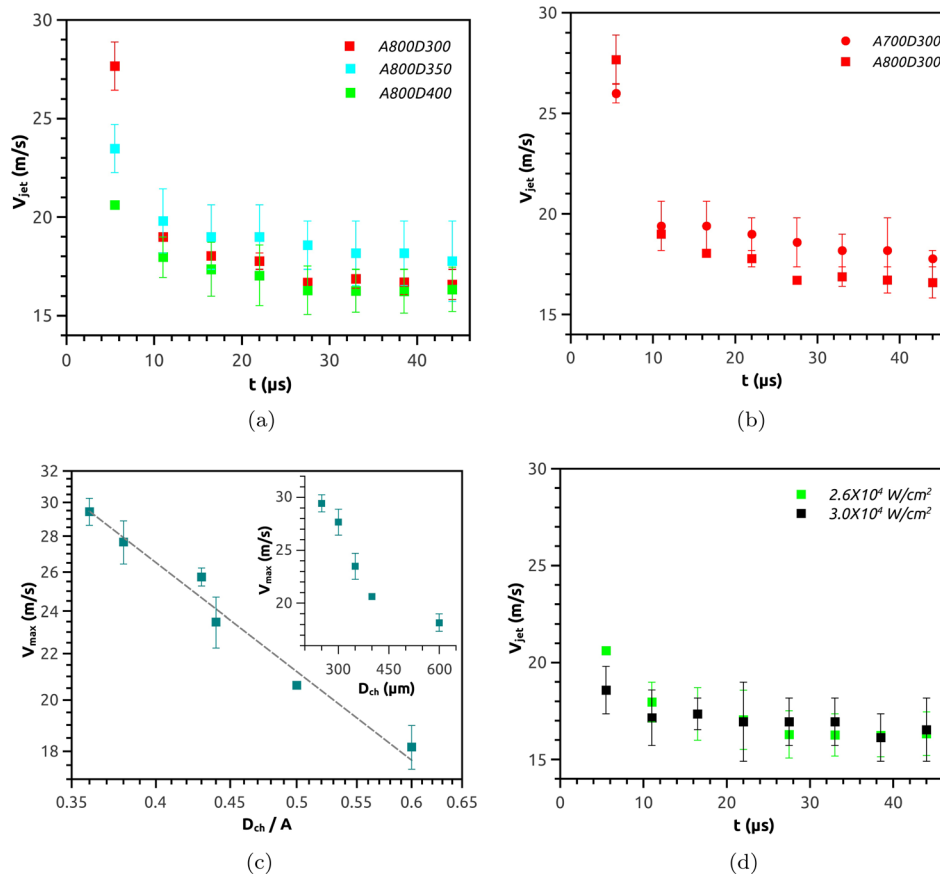


FIG. 5. Velocity of the jet for laser intensity $I = 2.6 \times 10^4$ W/cm², extracted from recorded images at 180 000 fps for: (a) Devices sharing same chamber size A800. (b) Devices sharing same channel size D300. (c) Maximum speed of the jet measured at $\sim 6 \mu$ s as a function of the constricted ratio $m = D/A$ (logarithmic scale). The dashed line shows a $V_{jet} = 10.6 m^{-1}$. The inset chart shows the maximum speed of the jet against channel diameter D_{ch} . (d) Jet velocity against time at $I = 2.6 \times 10^4$ W/cm² and 3×10^4 W/cm² for device A800D400.

mentioned in Section III A, the bubble expansion rate increases as the chamber width increases, leading therefore to a faster jet. This result indicates that the jet velocity not only depends on the channel diameter but it also depends on the chamber dimensions.

The maximum speed as function of channel diameter is plotted in the inset frame of Figure 5(c). A maximum speed of 29 m/s was reached for a diameter of 250 μ m, exceeding the velocity to produce skin erosion (13 m/s) (Ref. 27) by a factor of ~ 2 . In order to evaluate the combined effect of the channel diameter and the chamber width on the velocity of the jet, a dimensionless parameter named *constriction ratio* $m = D/A$ was defined. The velocity of the jet at different values of m is shown in Figure 5(c). As the constriction ratio is reduced, the velocity of the liquid increases. A data fitting curve shows a behavior of $V_{jet} = \alpha m^{-1}$, where $\alpha = 10.6 \pm 0.12$. This is similar to previous results,²⁴ where it was found a jet velocity proportional to D^{-1} for a given energy pulse in capillary tubes with diameters bigger than 50 μ m.

The jet velocity for different laser intensities of the device A800D400 is shown in Figure 5(d). At $I = 2.6 \times 10^4$ W/cm² ($P = 116$ mW and beam waist of 17 μ m), the jet reached a maximum velocity around 21 m/s; when the intensity was increased to 3×10^4 W/cm² ($P = 150$ mW and beam waist of 17 μ m) the velocity dropped to 19 m/s. This is remarkable since for pulsed lasers a linear dependence with the energy pulse was found.²⁴ A future study of the jet velocity as a function of laser intensity would be therefore highly interesting.

The jet velocities measured with this microfluidic device are still below those obtained by pulsed laser systems, but of comparable order of magnitude. For example, using an Er:YAG

laser, jet velocities up to 50 m/s were reached for a nozzle diameter of 150 μm with a pulse energy of 950 mJ.²⁷ With a Nd:YAG laser, jet velocities of 70 m/s were reached with the same nozzle diameter.²⁸ It is expected that the physical mechanisms (energy conversion from light into vapor, from vapor into motion, and flow focusing) leading to the jet expulsion are scale-invariant, as was demonstrated for a closely related case.²⁴ By extrapolating the curve in Figure 5(c), velocities around 100 m/s for $m = 0.1$ are predicted.

The results in this work show the potential of needle-free injection by using CW lasers. In future work, CW lasers with different wavelengths could be used to avoid the need of a light-absorbing dye. In particular, for wavelengths between 3 μm and 100 μm , the optical absorption coefficient is comparable to or shorter than $\sim 130 \text{ cm}^{-1}$, as used here. Furthermore, this investigation shows that smaller channel diameters likely yield higher jet velocities, to enable medicine delivery at controlled depths in the skin or the subcutaneous tissue. We believe that this approach to induce jets with CW lasers will eventually enable the development of commercially feasible, portable jet injectors.

IV. CONCLUSION

A glass-silicon microfluidic device for continuous wave laser generated jets was designed and tested. The system is integrated by a chamber, where the bubble expands, and a channel to focus the liquid jet through the exit. The bubble growth in the chamber is restricted to the channel diameter despite having more space to expand. However, a bubble growth rate proportional to the chamber width was found. As the bubble grows, it induces an elongated and focused jet that exits the microfluidic device through the channel which connects the chamber to the ambient air. The jet velocity was measured and found to follow a scaling $V_{jet} \sim m^{-1}$, where $m = \frac{D}{A}$ is the ratio between the chamber width and the channel diameter. Here, we observed maximal jet velocities of 29 m/s, which is sufficient to break the stratum corneum. However, in order to penetrate the skin dermis, further studies with new microfluidic designs will be needed to obtain higher jet speeds. Therefore, in future work, devices with lower values of m will be tested with the aim to enable velocities of up to 200 m/s, which are usually applied for needle-free injection drug.

ACKNOWLEDGMENTS

The authors acknowledge financial support from CONACyT-Mexico and are grateful to Prof. Detlef Lohse and Prof. Cha Sun from POF for their support, advice and access to their laboratory equipment. Also, a special thanks to Remco Sanders and Jeroen Korterik for laboratory assistance.

¹Y. Chartier, J. Emmanuel, U. Pieper, A. Prüss, P. Rushbrook, R. Stringer, W. Townend, S. Wilburn, and R. Zghondi, *Safe Management of Wastes from Health-Care Activities* (World Health Organization, 2014).

²S. Q. Wilburn and G. Eijkemans, "Preventing needlestick injuries among healthcare workers: A WHO-ICN Collaboration," *Int. J. Occup. Environ. Health* **10**, 451–456 (2004).

³Y. Guo, J. Shiao, Y. Chuang, and K. Huang, "Needlestick and sharps injuries among health-care workers in Taiwan," *Epidemiol. Infect.* **122**(2), 259–265 (1999).

⁴B. P. Lanphear, C. C. Linnemann, C. G. Cannon, M. M. DeRonde, L. Pendy, and L. M. Kerley, "Hepatitis C virus infection in healthcare workers: Risk of exposure and infection," *Infect. Control Hosp. Epidemiol.* **15**, 745–750 (1994).

⁵A. P. Raphael, O. R. L. Wright, H. A. Benson, and T. W. Prow, "Recent advances in physical delivery enhancement of topical drugs," *Curr. Pharm. Des.* **21**, 2830–2847 (2015).

⁶J. Schramm-Baxter and S. Mitragotri, "Needle-free jet injections: Dependence of jet penetration and dispersion in the skin on jet power," *J. Controlled Release* **97**, 527–535 (2004).

⁷A. Adamo, O. Roushdy, R. Dokov, A. Sharei, and K. F. Jensen, "Microfluidic jet injection for delivering macromolecules into cells," *J. Micromech. Microeng.* **23**, 035026 (2013).

⁸A. Arora, I. Hakim, J. Baxter, R. Rathnasingham, R. Srinivasan, D. A. Fletcher, and S. Mitragotri, "Needle-free delivery of macromolecules across the skin by nanoliter-volume pulsed microjets," *Proc. Natl. Acad. Sci. U.S.A.* **104**, 4255–4260 (2007).

⁹N. C. Hogan, B. D. Hemond, D. M. Wendell, A. J. Taberner, and I. W. Hunter, "Delivery of active collagenase to skin using a lorentz-force actuated needle-free injector," in *Annual International Conference of the IEEE Engineering in Medicine and Biology Society* (2006), Vol. 1, pp. 5611–5616.

¹⁰J. C. Stachowiak, T. H. Li, A. Arora, S. Mitragotri, and D. A. Fletcher, "Dynamic control of needle-free jet injection," *J. Controlled Release* **135**, 104–112 (2009).

- ¹¹C. M. G. J. Houtzagers, A. P. Visser, P. A. Berntzen, R. J. Heine, and E. A. Veen, "The Medi-Jector II: Efficacy and acceptability in insulin-dependent diabetic patients with and without needle phobia," *Diabetic Med.* **5**, 135–138 (1988).
- ¹²A. Taberner, N. C. Hogan, and I. W. Hunter, "Needle-free jet injection using real-time controlled linear Lorentz-force actuators," *Med. Eng. Phys.* **34**, 1228–1235 (2012).
- ¹³M. Kendall, T. Mitchell, and P. Wrighton-Smith, "Intradermal ballistic delivery of micro-particles into excised human skin for pharmaceutical applications," *J. Biomech.* **37**, 1733–1741 (2004).
- ¹⁴M. Kendall, "Engineering of needle-free physical methods to target epidermal cells for DNA vaccination," *Vaccine* **24**, 4651–4656 (2006).
- ¹⁵J. Myschik, W. T. McBurney, T. Hennessy, T. Rades, and S. Hook, *Pharm. - Int. J. Pharm. Sci.* **63**(9), 686 (2008).
- ¹⁶A. C. Sintov, I. Krymberk, D. Daniel, T. Hannan, Z. Sohn, and G. Levin, "Radiofrequency-driven skin microchanneling as a new way for electrically assisted transdermal delivery of hydrophilic drugs," *J. Controlled Release* **89**, 311–320 (2003).
- ¹⁷G. Levin, A. Gershonowitz, H. Sacks, M. Stern, A. Sherman, S. Rudaev, I. Zivin, and M. Phillip, "Transdermal delivery of human growth hormone through RF-microchannels," *Pharm. Res.* **22**, 550–555 (2005).
- ¹⁸S. Mitragotri and J. Kost, "Low-frequency sonophoresis: A review," *Adv. Drug Delivery Rev.* **56**, 589–601 (2004).
- ¹⁹L. M. Strambini, A. Longo, A. Diligenti, and G. Barillaro, "A minimally invasive microchip for transdermal injection/sampling applications," *Lab Chip* **12**, 3370–3379 (2012).
- ²⁰R. K. Sivamani, D. Liepmann, and H. I. Maibach, "Microneedles and transdermal applications," *Expert Opin. Drug Delivery* **4**, 19–25 (2007).
- ²¹D. V. McAllister, M. G. Allen, and M. R. Prausnitz, "Microfabricated microneedles for gene and drug delivery," *Annu. Rev. Biomed. Eng.* **2**, 289–313 (2000).
- ²²A. Arora, M. R. Prausnitz, and S. Mitragotri, "Micro-scale devices for transdermal drug delivery," *Int. J. Pharm.* **364**, 227–236 (2008).
- ²³C. Pegoraro, S. MacNeil, and G. Battaglia, "Transdermal drug delivery: From micro to nano," *Nanoscale* **4**, 1881–1894 (2012).
- ²⁴Y. Tagawa, N. Oudalov, C. W. Visser, I. R. Peters, D. van der Meer, C. Sun, A. Prosperetti, and D. Lohse, "Highly focused supersonic microjets," *Phys. Rev. X* **2**, 031002 (2012).
- ²⁵Y. Tagawa, N. Oudalov, A. El Ghalbzouri, C. Sun, and D. Lohse, "Needle-free injection into skin and soft matter with highly focused microjets," *Lab Chip* **13**, 1357–1363 (2013).
- ²⁶T. Han and J. J. Yoh, "A laser based reusable microjet injector for transdermal drug delivery," *J. Appl. Phys.* **107**, 103110 (2010).
- ²⁷M. Park, H. Jang, F. V. Sirotkin, and J. J. Yoh, "Er:YAG laser pulse for small-dose splashback-free microjet transdermal drug delivery," *Opt. Lett.* **37**, 3894 (2012).
- ²⁸H. Jang, M. Park, F. V. Sirotkin, and J. J. Yoh, "Laser-induced microjet: Wavelength and pulse duration effects on bubble and jet generation for drug injection," *Appl. Phys. B* **113**, 417–421 (2013).
- ²⁹H. Jang, H. Yu, S. Lee, E. Hur, Y. Kim, S.-H. Lee, N. Kang, and J. J. Yoh, "Towards clinical use of a laser-induced microjet system aimed at reliable and safe drug delivery," *J. Biomed. Opt.* **19**, 058001 (2014).
- ³⁰T.-H. Han, J.-M. Hah, and J. J. Yoh, "Drug injection into fat tissue with a laser based microjet injector," *J. Appl. Phys.* **109**(9), 093105 (2011).
- ³¹J. P. Padilla-Martinez, J. C. Ramirez-San-Juan, N. Korneev, D. Banks, G. Aguilar, and R. Ramos-Garcia, "Breaking the Rayleigh-Plateau instability limit using thermocavitation within a droplet," *Atomization Sprays* **23**(6), 487–503 (2013).
- ³²D. Fernandez Rivas and J. G. E. Gardeniers, "On the resilience of PDMS microchannels after violent optical breakdown microbubble cavitation," in *6th International Conference on Nanochannels, Microchannels, and Minichannels* (ASME, 2008), Paper No. ICNMM2008-62385, pp. 1939–1942.
- ³³T.-H. Wu, L. Gao, Y. Chen, K. Wei, and P.-Y. Chiou, "Pulsed laser triggered high speed microfluidic switch," *Appl. Phys. Lett.* **93**, 144102 (2008).
- ³⁴S. F. Rastopov and A. T. Sukhodolsky, "Sound generation by thermocavitation induced CW-laser in solutions," *Proc. SPIE* **1440**, 127–134 (1991).
- ³⁵J. C. Ramirez-San-Juan, E. Rodriguez-Aboytes, A. E. Martinez-Canton, O. Baldovino-Pantaleon, A. Robledo-Martinez, N. Korneev, and R. Ramos-Garcia, "Time-resolved analysis of cavitation induced by CW lasers in absorbing liquids," *Opt. Express* **18**, 8735–8742 (2010).
- ³⁶P. A. Quinto-Su, K. Y. Lim, and C.-D. Ohl, "Cavitation bubble dynamics in microfluidic gaps of variable height," *Phys. Rev. E* **80**, 047301 (2009).